A Physically Transient Form of Silicon Electronics

Suk-Won Hwang *et al.*

Science **337**, 1640 (2012);
DOI: 10.1126/science.1226325

Science (print ISSN 0036-8075; online ISSN 1095-9203) is published weekly, except the last week in December, by the American Association for the Advancement of Science, 1200 New York Avenue NW, Washington, DC 20005.

by a 3 to 10% perturbation in the local rotation rate in the outer few percent of the Sun (*16*).

Finally, the Sun's mean hexadecapole shape amplitude is small (–0.1 ± 0.4 milli–arc sec) but shows a hint of variability (*21*). This value is marginally correlated with the sunspot cycle with an amplitude of 2.1 ± 2 milli–arc sec. The hexadecapole shape is also sensitive to the internal solar differential rotation, but if due only to rotation, it would require large changes (on the order of 50%) in the outer parts of the Sun (*16*) that are not consistent with the constant helioseismic rotation (*20*) and the constant oblateness. In contrast, solar-cycle changes in near-surface flows or magnetic stresses localized near mid-latitudes could affect C_4 and not the oblateness.

References and Notes

1. R. H. Dicke, *Nature* **202**, 432 (1964).
2. H. A. Hill, R. T. Stebbins, *Astrophys. J.* **200**, 477 (1975).
3. R. H. Dicke, J. R. Kuhn, K. G. Libbrecht, *Astrophys. J.* **318**, 451 (1987).
4. A. Egidi *et al.*, *Sol. Phys.* **235**, 407 (2006).
5. J. Rösch, J. P. Rozelot, H. Deslandes, V. Desnoux, *Sol. Phys.* **165**, 1 (1996).
6. C. Damiani, J. P. Rozelot, S. Lefebvre, A. Kilcik, A. G. Kosovichev, *J. Atmos. Sol. Terr. Phys.* **73**, 241 (2011).
7. M. Emilio, R. Bush, J. R. Kuhn, P. Scherrer, *Astrophys. J.* **660**, L161 (2007).
8. M. D. Fivian, H. S. Hudson, R. P. Lin, H. J. Zahid, *Science* **322**, 560 (2008).
9. J. P. Rozelot, C. Damiani, *Eur. Phys. J. H* **36**, 407 (2011).
10. J. R. Kuhn, R. I. Bush, X. Scheick, P. Scherrer *Nature* **392**, 155 (1998).
11. We let $L(r,\theta)$ be the observed LDF function from a binned satellite image. From this, we used the circular average mean LDF represented by $\Gamma(r)$ to solve for a brightness function $\alpha(\theta)$ and the limb shape $\beta(\theta)$. The binned LDF function was then expressed as $L(r,\theta) = [\alpha(\theta) + 1]\Gamma[r - \beta(\theta)]$, where α and β represent the mean limb brightness change and position around the limb. We then linearized this equation and solved it as a least-squares problem to find α and β. We obtained the function $\Gamma(r)$ from the binned intensity of limb pixels, whereas we iterated the solution for $\beta(\theta)$ so that $\Gamma(r)$ was adjusted at each iteration by correcting the limb-pixel binning by shifting pixels by the local $\beta(\theta)$ from the previous iteration. This was done for each of the typically 13,000 images obtained during an SDO spacecraft roll. After two iterations, the solution was stable to better than 5%.
12. J. Schou *et al.*, *Sol. Phys.* **275**, 229 (2012).
13. Figure S1 shows that the analysis recovers the limb shape, independent of any limb brightness variations. Figure S2 shows that independent simultaneous HMI solar-limb shape and brightness measurements agree on all angular scales and that the limb position and brightness measurements are dominated by solar atmosphere inhomogeneity and its global asphericity.
14. R. J. Bray, R. E. Loughheed, *Sunspots* (Wiley, New York, 1965).
15. Figure S3 shows how the limb brightness and position are correlated and how the brightness measurements [α, see (*11*)] can be used to flag localized magnetic limb contamination of the limb shape. The shape analysis is broadly insensitive to the brightness threshold, with no significant change in the derived global oblateness, even with large changes in the assumed brightness threshold.
16. J. D. Armstrong, J. R. Kuhn, *Astrophys. J.* **525**, 533 (1999).
17. The χ^2statistic for these 5 degrees of freedom and a constant to describe the Fig. 4 C_2 data are both equal to 2.8. This indicates no statistical basis for a nonconstant C_2 at better than the 99.9% confidence level.
18. J. R. Kuhn, M. Emilio, R. Bush, *Science* **324**, 1143 (2009).
19. R. I. Bush, M. Emilio, J. R. Kuhn, *Astrophys. J.* **716**, 1381 (2010).
20. R. Howe, *Living Rev. Sol. Phys.* **6**, 1 (2009).
21. The χ^2 statistic for describing the hexadecapole amplitude as a constant was 9.4. This was marginally inconsistent (at 95% level) with a constant. Linear regression of the hexadecapole measurements against the sunspot number time series suggested a marginally significant hexadecapole solar-cycle variation with an amplitude of 2.1 ± 2 milli–arc sec.

Acknowledgments: The raw and astrometric data used for this analysis are available via the HMI public archives (http://jsoc.stanford.edu). The development of the HMI astrometry pipeline was supported by NASA and a grant to Stanford Univ. and the Univ. of Hawaii (NNX09AI90G). The HMI experiment aboard the SDO satellite was funded, in part, by a NASA contract to Stanford (NAS5-02139). J.R.K. was supported by a senior Humboldt prize while some of this work was done at the Kiepenheuer Institut fur Sonnenphysik. M.E. was partially supported by Instituto Nacional de Estudos do Espaço (CNPq), CNPq grant 303873/2010-8, and Coordenação de Aperfeiçoamento de Pessoal de Nivel Superior grant 0873/11-0. We thank H. Hudson for comments on this manuscript.

Supplementary Materials

www.sciencemag.org/cgi/content/full/science.1223231/DC1
Supplementary Text
Figs. S1 to S3
Table S1
References

11 April 2012; accepted 7 August 2012
Published online 16 August 2012;
10.1126/science.1223231

A Physically Transient Form of Silicon Electronics

Suk-Won Hwang,[1]* Hu Tao,[2]* Dae-Hyeong Kim,[3]* Huanyu Cheng,[4] Jun-Kyul Song,[5] Elliott Rill,[1] Mark A. Brenckle,[2] Bruce Panilaitis,[2] Sang Min Won,[6] Yun-Soung Kim,[1] Young Min Song,[1] Ki Jun Yu,[6] Abid Ameen,[1] Rui Li,[4,7] Yewang Su,[4] Miaomiao Yang,[2] David L. Kaplan,[2] Mitchell R. Zakin,[8] Marvin J. Slepian,[9] Yonggang Huang,[4] Fiorenzo G. Omenetto,[2,10]† John A. Rogers[1,5,6]†

A remarkable feature of modern silicon electronics is its ability to remain physically invariant, almost indefinitely for practical purposes. Although this characteristic is a hallmark of applications of integrated circuits that exist today, there might be opportunities for systems that offer the opposite behavior, such as implantable devices that function for medically useful time frames but then completely disappear via resorption by the body. We report a set of materials, manufacturing schemes, device components, and theoretical design tools for a silicon-based complementary metal oxide semiconductor (CMOS) technology that has this type of transient behavior, together with integrated sensors, actuators, power supply systems, and wireless control strategies. An implantable transient device that acts as a programmable nonantibiotic bacteriocide provides a system-level example.

An overarching goal in the development of nearly any new class of electronics is to achieve high-performance operation in physical forms that undergo negligible change with time. Active and passive materials, device and circuit layouts, and packaging strategies are each formulated individually and then configured collectively to accomplish this outcome. Here we present concepts and strategies for electronics that involve similar attention to engineering designs, but with the goal of achieving systems that physically disappear at prescribed times and at controlled rates. Applications that could exploit this transient behavior include implantable medical diagnostic and therapeutic devices that resorb in the body to avoid adverse long-term effects, fieldable environmental sensors that dissolve to eliminate the need for their retrieval, and portable consumer devices that decompose to minimize the costs and health risks associated with recycling and the management of hazardous waste streams. For these three examples, the desired time scales for transience range from days or weeks, to months, to years, respectively. The approaches reported here can address these and other application concepts with circuit components whose operational characteristics match those of nontransient counterparts formed in the usual way on silicon wafer substrates. When combined with transient sensors, actuators, power supplies, and wireless control systems, this technology provides levels of function that substantially exceed those available

[1]Department of Materials Science and Engineering, Beckman Institute for Advanced Science and Technology, and Frederick Seitz Materials Research Laboratory, University of Illinois at Urbana–Champaign, Urbana, IL 61801, USA. [2]Department of Biomedical Engineering, Tufts University, Medford, MA 02155, USA. [3]School of Chemical and Biological Engineering, Center for Nanoparticle Research of Institute for Basic Science, WCU Program of Chemical Convergence for Energy and Environment, Seoul National University, Seoul 151-741, Republic of Korea. [4]Department of Mechanical Engineering and Department of Civil and Environmental Engineering, Northwestern University, Evanston, IL 60208, USA. [5]Department of Chemistry, University of Illinois at Urbana–Champaign, Urbana, IL 61801, USA. [6]Department of Electrical and Computer Engineering, University of Illinois at Urbana–Champaign, Urbana, IL 61801, USA. [7]State Key Laboratory of Structural Analysis for Industrial Equipment, Department of Engineering Mechanics, Dalian University of Technology, Dalian 116024, China. [8]Nano Terra, Brighton, MA 02135, USA. [9]Department of Medicine and Department of BioMedical Engineering, Sarver Heart Center, University of Arizona, Tucson, AZ 85724, USA. [10]Department of Physics, Tufts University, Medford, MA 02155, USA.

*These authors contributed equally to this work.
†To whom correspondence should be addressed. E-mail: jrogers@uiuc.edu (J.A.R.); fiorenzo.omenetto@tufts.edu (F.G.O.)

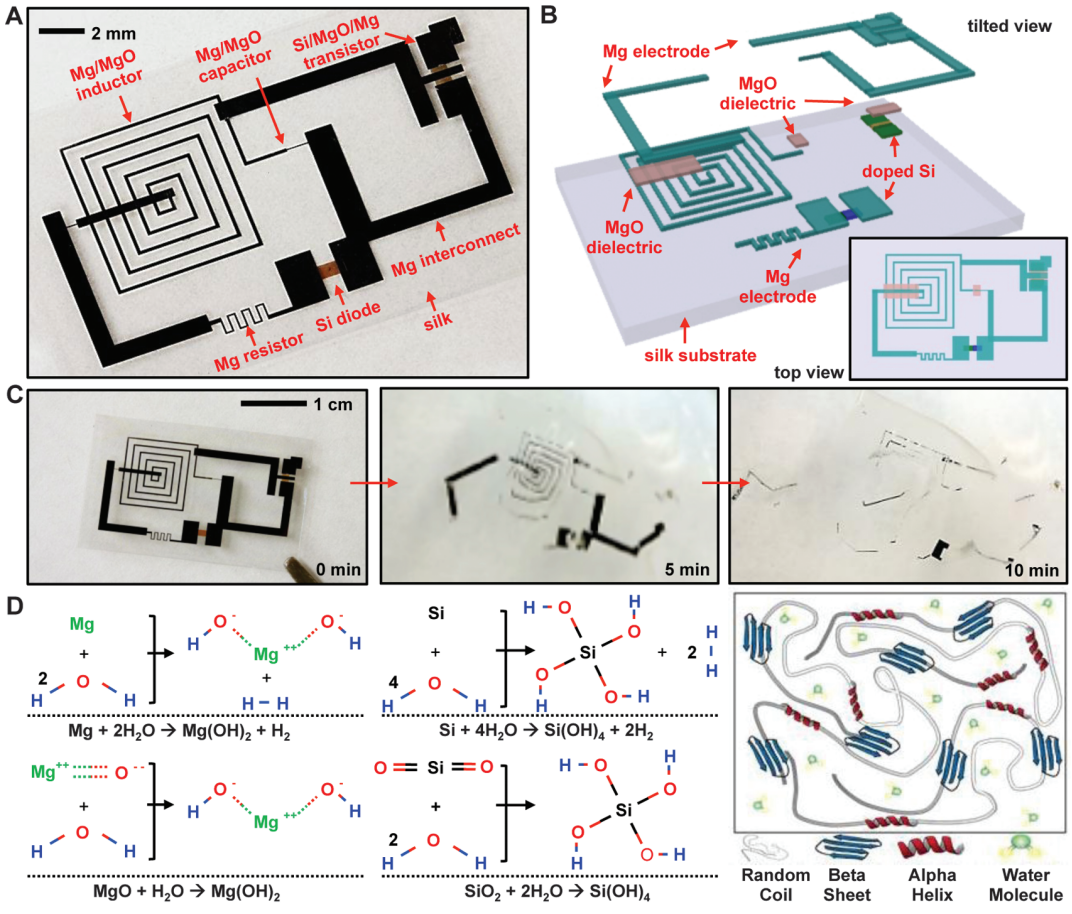

Fig. 1. Demonstration platform for transient electronics, with key materials, device structures, and reaction mechanisms. (**A**) Image of a device that includes transistors, diodes, inductors, capacitors, and resistors, with interconnects and interlayer dielectrics, all on a thin silk substrate. (**B**) Exploded-view schematic illustration, with a top view in the lower right inset. (**C**) Images showing the time sequence of dissolution in DI water. (**D**) Chemical reactions for each of the constituent materials with water.

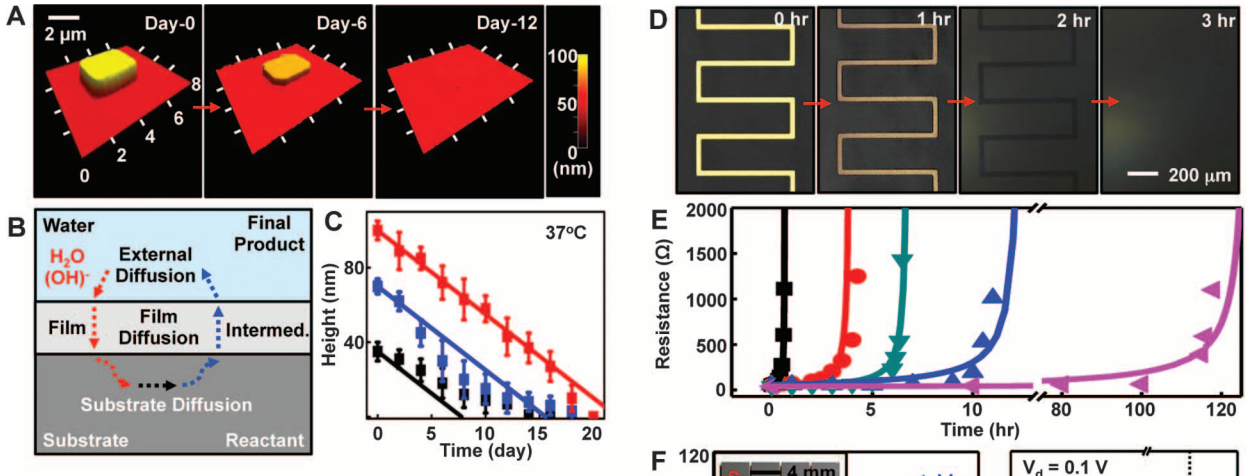

Fig. 2. Experimental studies of transient electronic materials and devices and corresponding theoretical analysis. (**A**) Atomic force microscope topographical images of a Si NM (initial dimensions: 3 μm × 3 μm × 70 nm) at various stages of hydrolysis in PBS at 37°C. (**B**) Diagram of the processes of reactive diffusion used in models of transience. (**C**) Experimental (symbols) and theoretical (lines) results for time-dependent dissolution of Si NMs (35 nm, black; 70 nm, blue; 100 nm, red) in PBS at 37°C. (**D**) Optical microscope images of the dissolution of a serpentine trace of Mg (150 nm thick) on top of a layer of MgO (10 nm thick) in DI water at room temperature. (**E**) Experimental (symbols) and theoretical (lines) results of dissolution kinetics of similar traces of Mg (300 nm thick) with different encapsulating layers: MgO (400 nm, red; 800 nm, blue) and silk (condition i, cyan; condition ii, purple). (**F**) Measurements of transience in operational characteristics of n-channel transistors encapsulated by MgO and crystallized silk (picture in the inset on the left) and then immersed in DI water. The results show the drain current (I_d) at V_d = 0.1 V as a function of V_g at various times (left) and at V_g = 5 V as a function of time (right).